COB-2023-0702

RESIDUAL STRESS EVALUATION IN OVERLAP JOINTS PRODUCED WITH LBW AND GTAW PROCESSES IN AISI 316L STAINLESS STEEL

Felipe Soares Fundão
Massimo Freitas Nodari Cruz
Rogério Lima Mota de Oliveira
Sheila Medeiros de Carvalho
Olga Liskevych

Federal University of Espirito Santo, Vitoria – Brazil

e-mail: felipe_fundao@hotmail.com, massimo.cruz@edu.ufes.br, rogerio.mota@eb.mil.br, sheila.m.carvalho@ufes.br, olga.liskevych@ufes.br

Abstract. *Residual stress evaluation in welded joints is of major importance, since its underestimation or lack of control can lead to deformations of welded components, to its mechanical properties´ deterioration or even to failure in service, for example, when there is a tensile stress overlay beyond the yield stress limit. What concerns overlap type of joints, widely used in the automotive and petrochemical industries, tensile residual stress presence due to great thermal gradients and geometrical complexity of the structure may also contribute to the appearance of corrosion cracks. The objective of this study was to evaluate the residual stress distribution in overlap joints produced from stainless austenitic steel AISI 316L using different types of welding heat sources. Thus, 0.9 mm thick samples were welded with LBW and GTAW welding processes after defying the optimum parameter conditions for each procedure based on penetration efficiency and absence of defects. Subsequently, the longitudinal and transversal components of the residual stress induced by the joining procedure were measured using the ESPI-based hole-drilling method up to 0.4 mm depth at the top and root of the resultant joints. This methodology allowed the evaluation of residual stress distribution in each sample, taking into account fusion and heat effected zones, as well as base metal values. The residual stress distribution results were consistent with the theoretical models for both processes. The longitudinal component in the LBW sample showed the best repeatability of measurements and the lowest standard deviation, which may be associated to the weld geometry and heterogeneity. The tensile stress intensity was reported to be the highest in the heat effected zone of the GTAW produced sample, reaching 76% of the yield tensile strength of the AISI 316L. The difference between the residual stress at the top and at the root of the welds was reported for the GTAW produced sample and was a consequence of the partial penetration of the weld.*

Keywords: *residual stress, overlap joint, AISI 316L, LBW, GTAW*

1. INTRODUCTION

Residual stress (RS) is defined as the elastic stress that remains in a component when all external forces and/or temperature gradients are removed, according to Lu (1996). Virtually all mechanical components are subjected to these internal stresses, which are highly relevant phenomena in the field of engineering.

In fusion welding, RS is primarily caused by thermal stresses owing to compressive yielding that occurs around the molten zone as the material heats and expands during the process. When the weld metal cools, it contracts, causing tensile stresses, particularly in the longitudinal direction, as shown in Fig. 1 (a). After welding, the residual tensile stress remains across the weld centerline and causes a balancing compressive stress further from the weld zone, as shown in the model of Fig. 1 (b), where longitudinal and transversal components are referred as σ_y and σ_x, correspondingly.

The resultant stresses can have both beneficial and detrimental effects on the performance of welded mechanical elements, as their presence influences dimensional stability and component distortions (Colegrove et al., 2009; Vasantharaja et al., 2012; Gannon et al., 2010), fatigue resistance (Edwards, 2006; Barsoum & Barsoum, 2009; Haohui et al., 2021), hot cracking occurrence (Hagenlocher, 2020), among other factors. For example, compressive stresses tend to be beneficial because they generally inhibit cracking nucleation and/or propagation by counteracting slip lines caused by the movement of dislocations in the crystal lattice of the metal. On the other hand, tensile stresses can be detrimental; for example, when the tensile RS provoked by the welding procedure adds up the tensile stresses already present in the welded piece, premature failure of the component may occur, since this condition favors the initiation and growth of fatigue cracks, leading to material instability and rupture.

There is a bunch of aspects that influence the thermal stress and consequent RS generation in welded joints, such as welding energy and type of the heat source, material properties and its thickness, pre-heating, etc. In their extensive review

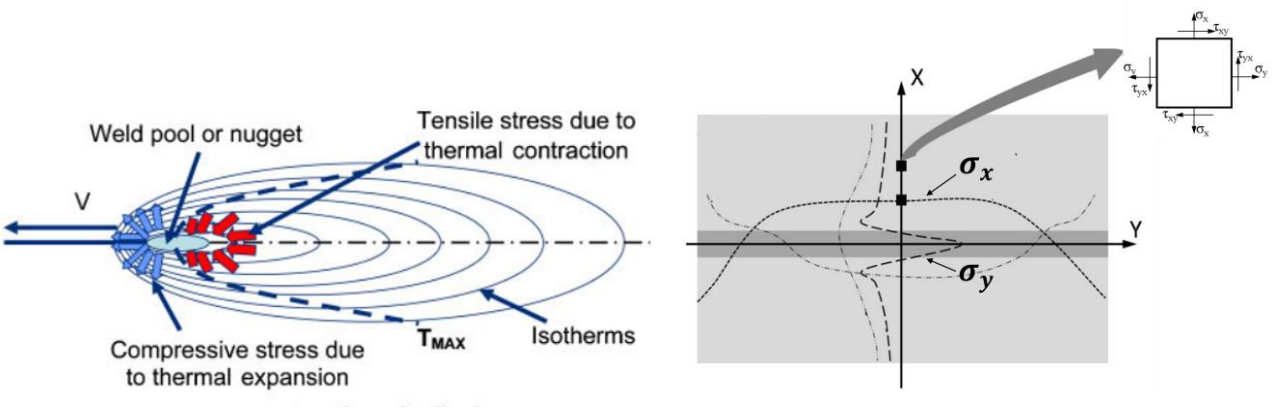

(a) (b)

Figure 1. Thermal stress in fusion welding: (a) thermal stresses during the process (Colegrove et al., 2009); (b) residual longitudinal σ_y and transversal σ_x stress in welded component (modified form Mishchenko and Scotti (2018))

of the impact of welding parameters on RS, Mischenko and Scotti (2018) established three main factors of major importance (so-called primer parameters): the cooling rate of the welded metal, metallurgical transformations, and the volume of the heated material. Yet the authors state that there are some controversial results in the current literature regarding the impact of these factors on RS generation and provide some examples.

While metallurgical transformations should be analyzed for each specific material and its chemical composition separately, increasing the cooling rate has been shown to generate a lower RS, according to Kumar et al. (2017). However, conflicting results were reported by Jones and Alberry (1978). The application of preheating has been found to generate more intensive RS, according to Lin and Lee (1997), Satoh et al. (1975), Schroepfer and Kannengiesser (2014), and Schroepfer et al. (2017). However, there are conflicting results reported by Heinze et al. (2012a), Lee et al. (2012), and Lee (2007). The application of forced cooling has been shown to relieve RS in the base metal, as stated by Sudheesh and Prasad (2011). On the other hand, the same authors mentioned a negligible effect of forced cooling on RS in the fusion and heat effected zones. Still, different results regarding the influence of forced cooling have been obtained by Jiang et al. (2012). The authors observed a decrease in the maximum longitudinal RS in the fusion and heat effected zones, as well as an increase in the regions remote from the weld bead when forced cooling was applied.

What regards to volume of the heated material, it can be understood that the greater it is, the greater is the material contraction during cooling, which leads to the generation of the thermal stresses. The total heated volume is generally governed by the geometric parameters of the welded joint and is composed of the volume of the filler metal deposited in the groove and melted base metal (forming the fusion zone) and the volume of the base metal heated by the heat source (forming the heat effected zone). The volume of the deposited metal, in turn, depends on the geometry and dimensions of the groove, while the volume of the melted and heated metal depends on the welding process used and the plate thickness. As for the last one, increasing the plate thickness has been found to generate more RS, according to Teng et al. (2002) and Vakili-Tahami and Sorkhabi (2009).

In its turn, welding process and operational parameters have a significant influence on the RS generation. High heat input and slow cooling rates have been associated with increased residual stresses, as reported by Masubuchi (1980), Teng et al. (2002), and Vakili-Tahami and Sorkhabi (2009). Conversely, low heat input and rapid cooling rates have been found to result in reduced residual stresses, as mentioned by Lin and Lee (1997), Colegrove et al. (2009), and Xu et al. (2014).

Considering the factors described above, the objective of this study was to investigate RS generation in welding joints produced by two particular processes: LBW and GTAW, both of which are widely used in industry and are well known for their capacity of good quality welds. In order to fulfill the lack of information regarding a variety of welding joints in research publications (usually focused on butt and tee joints), an overlap configuration was used to AISI 316L steel samples. The methodology applied in this study allowed the evaluation of the RS distribution in each sample taking into account fusion and heat effected zones, as well as base metal values.

2. METHODOLOGY

AISI 316L stainless steel samples with 0.9 mm thickness were used for the purpose of this study. This structural material was chosen, in the first place, due to its extensive usage in many industrial fields, such as the nuclear, cryogenic, and shipbuilding industries and, also, due to its possibility of hot cracking and low corrosion resistance associated with

the welding. Thereby, a systematic and comprehensive study of RS generation in this material certainly contributes to the improvement of welding technology. The ultimate tensile strength, yield tensile strength, and elongation of the material used were 660 MPa, 300 MPa, and 69%, respectively. The chemical composition of the material is shown in Table 1.

Table 1. Chemical composition of AISI 316L (wt.%).

C	Si	P	S	Cr	Ni	Mo	Cu
0.021	0.77	0.039	0.001	16.92	12.16	2.03	0.20

Overlap joints, illustrated in Fig. 2 (b), were produced with the LBW and GTAW procedures, both autogenous. These welding processes were chosen for two major reasons. First, neither of them requires a filler material in this modality, which helps to eliminate the influence of the additional melted metal on RS generation, giving precedence only to the melted base metal (FZ) and the volume of the base metal heated by the heat source (HAZ). Furthermore, using these two processes allows the investigation of the welding energy and cooling rate influence on the RS in welded joints, since GTAW provides higher welding energy (due to lower travel speed) and consequently lower cooling rate, while LBW comes up with low welding energy (due to considerably higher travel speed) and faster cooling rate owing to its concentrated heat source.

Series of welds were carried out for each process in order to select the optimized welding parameters. The criteria for the selection of definitive samples were good bead penetration (to guarantee sufficient weldment resistance), adequate capping and smooth bead appearance, absence of surface defects such as undercuts, porosity, and superficial cracks. More details regarding the selection methodology and applied welding procedures can be found in Cruz (2022) and Fundão (2022). Thus, definitive samples welded with the LBW process were produced employing 2 kW laser (IPG, YLR-2000 Model) with a wavelength of 1.07 µm and a beam diameter of 100 µm. The procedure was carried out without a shielding gas, and the laser power and welding speed were maintained at 400 W and 50 mm/s, respectively. The GTAW process was carried out using a welding current at the range of 200 A, voltage of 10 V and travel speed of 7.0 mm/s. Pure argon was used as the shielding atmosphere, at a flow rate of 5 l/min. The calculated welding energies for the definitive weldments were 28 J/mm for the LBW procedure and 285 J/mm for the GTAW one.

After welding the definitive samples, the RS was measured in the resulting welds using the ESPI-based hole-drilling method. The equipment used in this study is shown in Fig. 2 (b) and consists of a camera for image capture, drilling tool, sample fixture device and laser beam with all its known properties. This beam is divided into two parts: the first is launched on the sample and reflected to the camera, while the second (referred to as the reference beam) passes through a piezoelectric phase change system and is subsequently directed to the same optical device. When a hole is drilled in a welded sample and the stress induced by the welding procedure is relieved by local deformation, the light beam reflected from the surface of the sample changes its characteristics. When compared to the reference beam, the reflected beam exhibits a phase shift, which leads to a new grain pattern (pixels) in the recorded camera images. From the difference in pixel arrangement before and after drilling, that is, before and after stress relief, a speckle pattern is obtained. Subsequently, the spackle patterns are processed as digital interferograms with an equipment algorithm, as demonstrated by Steinzig and Ponslet (2003), in order to obtain the local surface displacements caused by the machining of the sample and the corresponding RS present in the material before drilling.

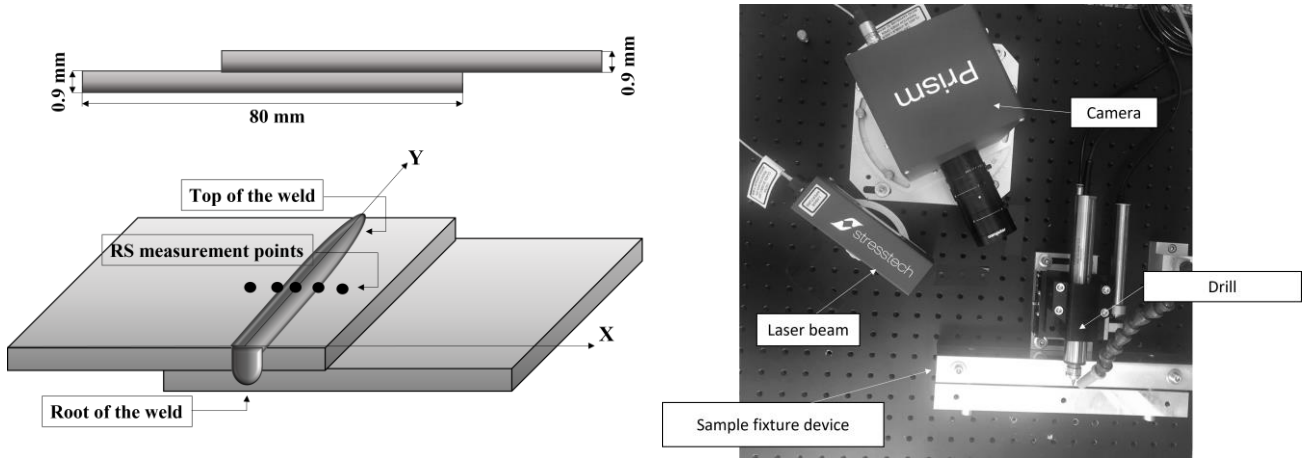

Figure 2. Residual stress measurement in LBW and GTAW produced samples: a) measurement in different weld bead areas of the overlap joint, (b) equipment arrangement for applied ESPI-based hole-drilling method.

The equipment described aforehand was calibrated using a standard four-point bending device and strip specimen with known properties, according to ASTM (2000) recommendations, demonstrating a 5.8% mean measurement error associated with the measurement uncertainties of the plunge indicator, elasticity modulus variation of material, as well as, with the error sources of the equipment itself. More details regarding the calibration procedure and its results can be found in the research conducted by Liskevych et al. (2022).

For both LBW and GTAW produced samples, series of RS measurements were carried out drilling 0.8 mm diameter hole at a rotational speed of 25000 rpm and 0.05 mm/s feed rate reaching the maximum hole depth of 0.4 mm (parameters previously tested by Upshaw et al. (2014) and Barile et al. (2014)). During machining, at each of 0.05 mm drilling increment, images were captured with interferometry pattern shifts owing to the changes occurring in the stress state of the material. After interferogram processing, the values of the measured stress in the longitudinal (σ_y) and transversal (σ_x) directions were provided for further analysis, along with the rate of poor pixels detected on the captured images. It is worth mentioning that in this study, longitudinal direction of the stress distribution (σ_y) was considered to be parallel to the weld bead position (see Fig. 1 (b)). Normally, major magnitude stress values are determined for this direction in materials that have experimented local fusion, due to higher temperature gradients and restriction levels. Transversal RS (σ_x) component, responsible for angular deformation in welded pieces, was considered to be perpendicular to the weld bead position (see Fig. 1 (b)).

In both definitive samples (welded with LBW and GTAW processes), RS measurements were performed in the base metal (BM) and fusion zone (FZ), as illustrated in Fig. 2 (a). Moreover, hole-drilling tests also were performed in the fusion line zone (FLZ) of the LBW sample and heat affected zone (HAZ) of the GTAW sample. Measurements were taken on the top of the weld beads and on their roots. For each measurement point, 3 tests were carried out in order to estimate repeatability of the results.

After the RS measurements the samples were cut, embedded, grinded, polished, and chemically etched with oxalic acid for further metallographic analysis. Afterwards, microhardness measurement tests were conducted using a 0.2 kg load which was applied for 10 s. Measurements were taken on the base metal (BM), in the quantity of 10, and fusion zone (FZ), in the quantity of 5, summarizing 15 indentations for each sample.

3. RESULTS AND DISCUSSION

The transverse cross-section and microstructure of the definitive AISI 316L overlap joints welded with the LBW and GTAW processes are shown in Fig. 3 and 4, respectively. No obvious defects such as porosity or hot cracking were observed. In both cases, the BM area mainly consisted of equiaxed austenite grains, and the FZ area mainly consisted of an austenite matrix decorated by skeletal δ-ferrite. This type of microstructure strongly depends on the solidification route; thus, it is expected that the LBW specimen (solidified with higher cooling rate) would result in a higher ferrite amount when compared to the GTAW joint. Similar microstructures have already been observed in AISI 316 L joints welded using both processes by Feng et al. (2015) and Zareie Rajani et al. (2012).

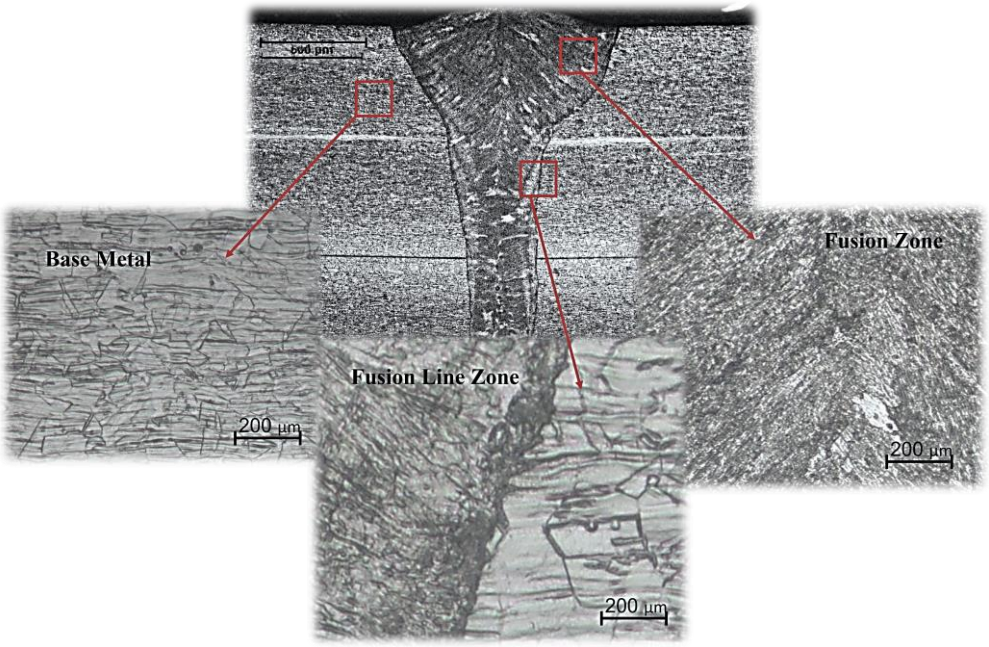

Figure 3. Transverse cross-section and microstructure of the AISI 316 L overlap joint welded with LBW process.

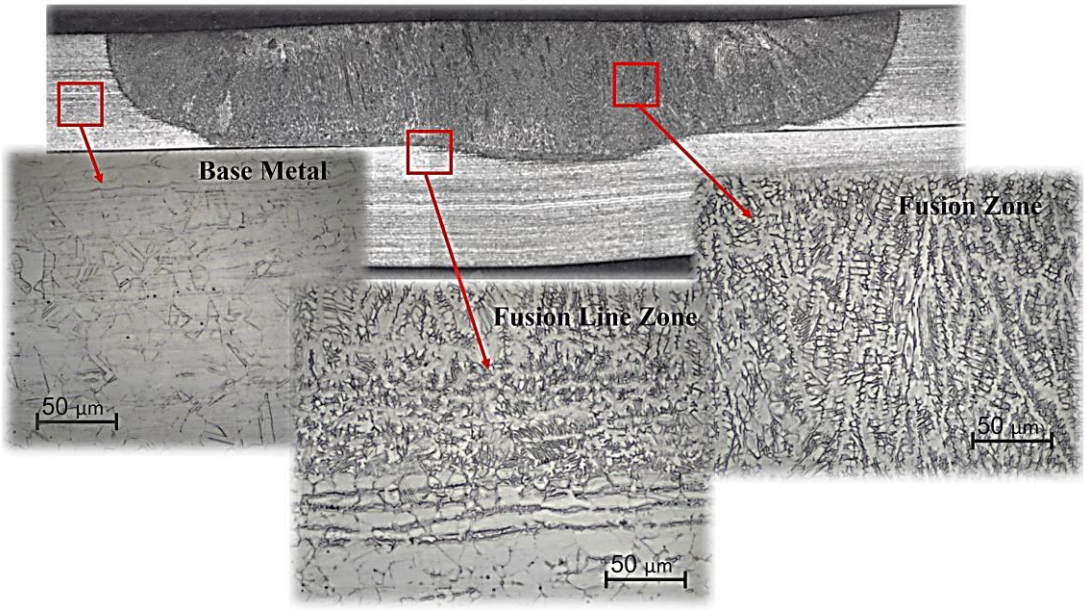

Figure 4. Transverse cross-section and microstructure of the AISI 316 L overlap joint welded with GTAW process.

As also expected, the bead geometry was different for both the studied cases because of the different heat source types applied during welding (concentrated laser beam vs. large-diameter arc). Both FZ and HAZ are much smaller in the LBW case compared to GTAW (maximum penetration and fusion area were calculated being 1.8 mm and 9.8 mm^2 for LBW and 1.5 mm and 11.2 mm^2 for GTAW produced samples).

As for the hardness of the analyzed welds, its Vickers values are shown in Fig. 5. In both cases, the values were higher in the FZ than in the BM, which was expected since the hardness of the material is affected by the microstructure, phase, and grain size. Thus, the presence of ferrite (hardness of which is higher than that of austenite) and finer dendritic structure (hardness of which is higher than that of equiaxed grains in the base metal) in the FZ could collaborate with this result, as also observed by Feng et al. (2015).

The hardness in the BM resulted in similar average values, that is, 200±2 HV and 196±9 HV, for the joints welded with LBW and GTAW, respectively. Nonetheless, the mean hardness value for the FZ was 12 % higher for the weld produced with the LBW process (247±9 HV) than for the GTAW welded joint (220±2 HV). This difference can be explained by the higher cooling rates and higher amount of ferrite in the FZ of the LBW sample, according to Soltani and Tayebi (2018) research.

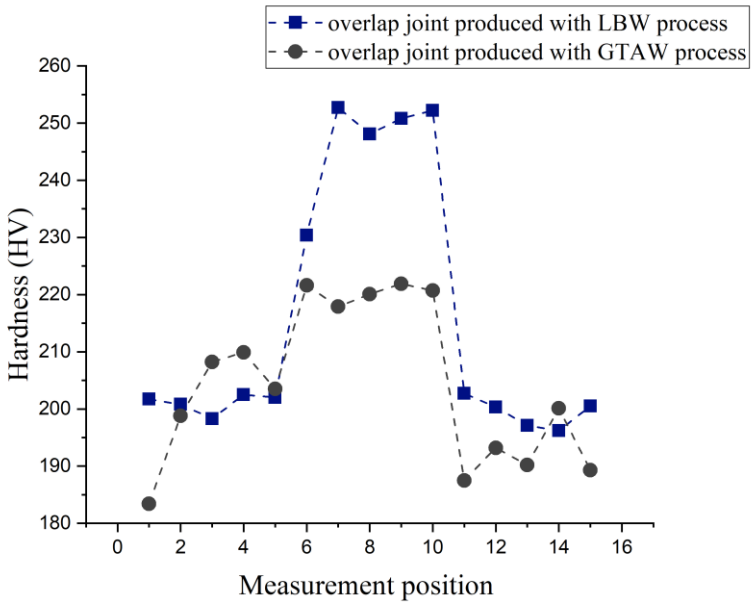

Figure 5. Hardness measured in the overlap joints produced by LBW and GTAW processes.

The results of the RS measurements carried out at the top and root of the weld are shown in Tables 2 and 3 for the overlap joint produced by the LBW process, and in Tables 4 and 5 for the overlap joint produced by the GTAW process. These are the mean values for the drilling intervals from 0.15 to 0.30 mm for 3 replicas of each measurement point (initial and final values were discarded taking into account methodology peculiarities discussed in Liskevych et al. (2022)). An illustration of the results can be found in Fig. 6 and Fig 7, respectively.

Table 2. Residual stress (MPa) measured at the top of the lap joint produced with the LBW process**.**

Test	Left side of the joint				FZ		Right side of the joint			
	BM		FLZ				FLZ		BM	
	σ_y	σ_x	σ_y	σ_x	σ_y	σ_x	σ_y	σ_x	σ_y	σ_x
1	-54.2	37.5	34.0	-12.2	96.4	14.7	44.5	5.9	-64.7	27.9
2	-67.0	26.1	39.2	3.7	107.2	10.1	49.1	-11.2	-52.2	19.3
3	-52.9	25.3	47.1	-9.4	103.7	8.0	40.2	-7.8	-62.7	21.5
Mean value	58.0	29.6	40.1	6.0	102.4	10.9	44.6	-4.4	-59.9	22.9
SD	7.8	6.8	6.6	8.5	5.5	3.4	4.5	9.1	6.7	4.5

Obs. BM – base metal, FLZ – fusion line zone of the LBW produced sample, FZ – fusion zone, (σ_y) – longitudinal residual stress, (σ_x) – transversal residual stress, SD – standard deviation.

Table 3. Residual stress (MPa) measured at the root of the lap joint produced with the LBW process**.**

Test	Left side of the joint				Fusion Zone		Right side of the joint			
	Base Metal		FLZ				FLZ		Base Metal	
	σ_y	σ_x	σ_y	σ_x	σ_y	σ_x	σ_y	σ_x	σ_y	σ_x
1	-49.7	17.2	44.8	4.8	110.2	6.5	51.2	-3.1	-60.2	19.9
2	-60.3	19.8	49.1	-3.7	103.1	16.3	47.7	-7.2	-52.8	19.3
3	-54.1	26.0	37.9	-10.1	103.6	18.2	43.5	-10.0	-59.1	23.1
Mean value	-54.7	21	43.9	-3	105.6	13.7	47.5	-6.8	57.4	20.8
SD	5.3	4.5	5.7	7.5	4.0	6.3	3.9	3.5	4.0	2.0

Obs. BM – base metal, FLZ – fusion line zone of the LBW produced sample, FZ – fusion zone, (σ_y) – longitudinal residual stress, (σ_x) – transversal residual stress, SD – standard deviation.

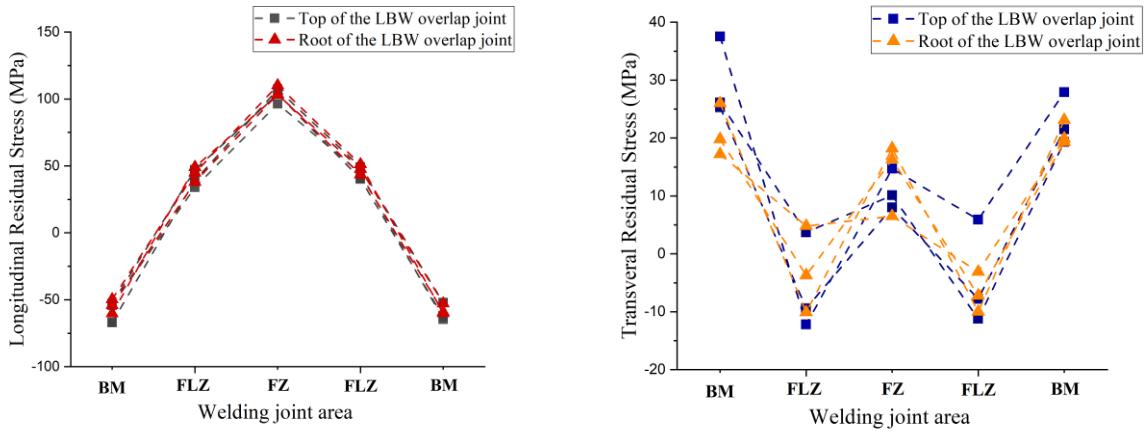

Figure 6. Longitudinal (σ_y) and transversal (σ_x) residual stress measured at the top and root of the overlap joint produced with the LBW process.

As for the RS measured in the overlap joint produced by the LBW process, it can be observed that the obtained longitudinal component values (σ_y) in Fig 6 have a good repeatability for all the weld areas and low standard deviation. Moreover, there was no significant difference between the values measured at the top and the root of the weld. In both cases, the longitudinal RS presented tensile values in the FZ and compressive values in the BM, in accordance with the theoretical models presented in the AWS Handbook (2001) and Scotti (2014). Differently, transversal RS (σ_x) (Fig. 6)

presented higher standard deviation of measurements, besides tensile values in the BM and null or compressive values in the FLZ. Alike in the case of the longitudinal component (σ_y), transversal RS (σ_x) in the FZ is reported to be tensile, nevertheless, of the significantly lower intensity. The differences in standard deviation can be explained by significant volume variations of the weld pool and consequent variations in the thermal stress and temperature gradient in the transverse direction when compared to the longitudinal one. The variation in the microstructure was also more pronounced in the transverse direction (see Fig. 3).

Table 4. Residual stress (MPa) measured at the top of the lap joint produced with the GTAW process**.**

Test	Left side of the joint				FZ		Right side of the joint			
	BM		HAZ				HAZ		BM	
	σ_y	σ_x	σ_y	σ_x	σ_y	σ_x	σ_y	σ_x	σ_y	σ_x
1	-109.7	129.8	346.0	-159.8	163.8	-75.4	194.3	-127.8	-121.5	113.9
2	-115.6	82.5	260.5	-175.8	227.8	-108.8	220.8	-125.3	-153.2	102.0
3	-144.2	103.5	283.8	-156.3	263.0	-12.2	188.0	-131.4	-143.8	96.0
Mean	-113.9	105.3	296.8	-163.2	218.2	-65.5	201.0	-128.5	-139.5	104.0
SD	18.5	23.7	44.2	10.4	50.3	49.1	17.4	3.1	16.3	9.1

Obs. BM – base metal, HAZ – heat affected zone of the GTAW produced sample, FZ – fusion zone, (σ_y) – longitudinal residual stress, (σ_x) – transversal residual stress, SD – standard deviation.

Table 5. Residual stress (MPa) measured at the root of the lap joint produced with the GTAW process**.**

Test	Left side of the joint				FZ		Right side of the joint			
	BM		HAZ				HAZ		BM	
	σ_y	σ_x	σ_y	σ_x	σ_y	σ_x	σ_y	σ_x	σ_y	σ_x
1	-120.9	154.0	184.3	-174.3	208.0	14.7	261.5	-25.6	-164.9	172.8
2	-124.2	157.3	241.8	-152.0	260.3	23.4	229.3	-80.0	-160.4	136.1
3	-107.1	82.3	260.8	-78.4	238.8	11.0	193.3	-116.7	-121.6	94.9
Mean	-117.4	131.2	228.9	-134.9	135.7	16.4	228.0	-74.00	-149.0	134.6
SD	9.1	42.4	39.8	50.2	26.3	6.4	34.1	45.8	23.8	39.0

Obs. BM – base metal, HAZ – heat affected zone of the GTAW produced sample, FZ – fusion zone, (σ_y) – longitudinal residual stress, (σ_x) – transversal residual stress, SD – standard deviation.

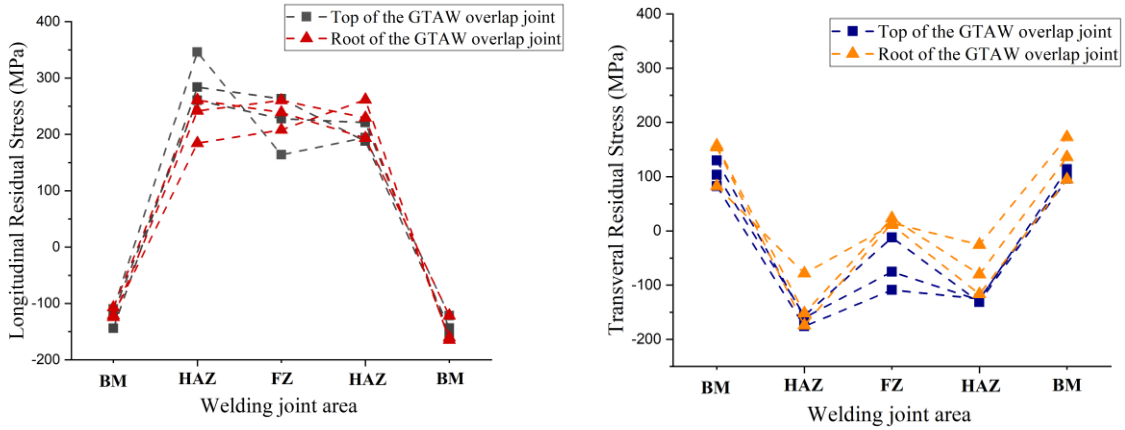

Figure 7. Longitudinal (σ_y) and transversal (σ_x) residual stress measured at the top and root of the overlap joint produced with the GTAW process.

Regarding the specimen produced with the GTAW process (see Fig. 7), both longitudinal (σ_y) and transversal (σ_x) RS values have higher standard deviation (especially in HAZ and FZ), either at the top or the root of the weld, when compared to the LBW produced joint. This can be related to the more pronounced plastic deformations observed in this weld owing to the slower cooling rates and greater melted and heated bead volume, as well as to the consequent structural heterogeneity of the GTAW welded specimen. Longitudinal component (σ_y) presented compressive values in the BM and tensile values both in the HAZ and FZ. However, there was no significant difference in the RS intensity between the HAZ

and FZ (contrary to the LBW welded sample). This tendency was observed for both the top and root of the weld, and it is in accordance with the conclusions of Colegrove et al. (2009) and Schroepfer and Kannengiesser (2014), who reported an increase in the longitudinal RS peak width when the welding energy was increased. Nevertheless, these authors also concluded that there was no difference between the maximum RS values when different welding energies were compared, which was not observed in this study (the longitudinal RS measured in the sample welded with a higher energy using the GTAW process presented higher values when compared to the LBW produced weld).

For the transversal component (σ_x), values of the RS measured in the BM and HAZ at the top and root of the overlap joint are quite similar (see Fig. 7), but the values measured in the FZ showed some difference. Thus, the transverse RS present in the FZ at the top of the weld was higher than the transverse RS present in the FZ at the root of the weld, which can be explained by the significant variation in the weld pool volume in the transverse direction (in accordance with the partial penetration shown in Fig. 4). Tensile values were reported for the BM, and compressive values were reported for the HAZ and FZ (a tendency similar to that of the LBW welded specimen).

For easier comprehension, the mean RS values from the Tabs. 2-5 (calculated for 3 replicas) for longitudinal (σ_y) and transversal (σ_x) components were plotted in Fig. 8. When analyzed on the same scale, the tensile longitudinal RS in the FZ and HAZ of the GTAW produced overlap joint appears to be higher than that of the LBW produced sample, for both the top and root of the weld. Indeed, the maximum tensile value in the HAZ was calculated to be 228 MPa, that is, 76% of the yield tensile strength of AISI 316L. Considering the already fragilized and significantly large HAZ in GTAW produced welds, this situation might be prejudicial for the joint in service.

Based on this result, the prevalence of the three main factors (so-called primer parameters) established by Mischenko and Scotti (2018) can be analyzed. Thus, considering a 12% reduction in the hardness and a 14% increase in the melted metal volume (FZ area) with an increase in welding energy (from 28 J/mm for the LBW procedure to 285 J/mm for the GTAW one), the maximum tensile RS in the FZ increased by approximately 114%, leading to the conclusion that the change in cooling rate was a major factor responsible for the intensity and format of the RS present in overlap joints welded with LBW and GTAW processes.

Transverse component (σ_x) showed similar behavior for the LBW produced joint and significant difference between the top and root areas for the GTAW produced sample (as the consequence of partial penetration weld in this case).

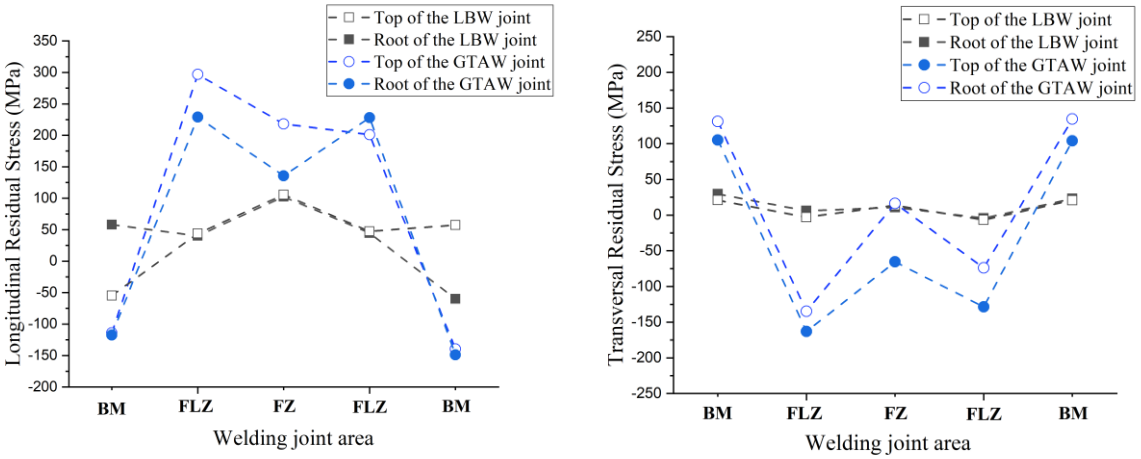

Figure 8. Mean values of the longitudinal and transversal residual stress measured at the top and root of the overlap joint produced with the LBW and GTAW processes.

4. CONCLUSIONS

The methodology applied in this study allowed the evaluation of the residual stress distribution in overlap joints produced with the LBW and GTAW processes, taking into account fusion and heat effected zones, as well as base metal values. Analyses were performed for the residual stress intensity and redistribution at the top and root of the welds. The resultant microstructure and hardness of the cross-sections were also considered. In both studied cases, the base metal area mainly consisted of equiaxed austenite grains, and the fusion zone area mainly consisted of an austenite matrix decorated by skeletal δ-ferrite, however, the concentrated heat source and higher cooling rates of the LBW process led to higher ferrite amount and, consequently, higher hardness when compared to the joint produced with GTAW.

The residual stress distribution presented results consistent with the theoretical models for both processes, even though the study was conducted over the overlap joints instead of the butt one. The longitudinal residual stress in the LBW sample showed the best repeatability of measurements and the lowest standard deviation, which might be associated to the weld geometry and heterogeneity. The tensile stress intensity was reported to be the highest in the heat effected zone of the

GTAW produced sample, reaching 76% of the yield tensile strength of the AISI 316L. For the transverse component, similar tendencies were observed for both LBW and GTAW: tensile values in the base metal and compressive values in the heat effected and fusion zones.

The difference between the residual stress reported for the top and root of the welds is a consequence of the penetration depth for both analyzed welds. Thus, full penetrated overlap joint produced with the LBW process practically did not show any difference in residual stress values measured at the top and root of the weld. In contrast, the partially penetrated overlap joint produced with the GTAW process resulted in residual stress variation, especially in the fusion zone.

5. ACKNOWLEDGEMENTS

The authors of this study would like to thank to LABENDEM of the Center of Research, Innovation and Development of the state of Espirito Santo, to the Laboratory of Metrology and TRICORMAT of the Federal University of Espirito Santo and to the FINEP project for the provided infrastructure and possibility of accomplishment of this work.

6. REFERENCES

ASTM, American Society for Testing of Materials, 2000. G39-99, *Standard practice for preparation and use of bent-beam stress-corrosion test specimens*.

AWS, American Welding Society, 2001. *Welding Handbook, Vol 1: Welding Technology, Chapter 7: Residual Stresses and Distortion*. 8º Edition, 891 p., ISBN: 0-87171-281-4.

Barile, C., Casavola, G., Pappalettere, G., and Pappalettere, C., 2014. "Analysis of the effects of process parameters in residual stress measurements on Titanium plates by HDM/ESPI". *Measurement*, Vol.: 48, pp. 220-227. Access: https://doi.org/10.1016/j.measurement.2013.11.014

Barsoum, Z. and Barsoum, I., 2009. "Residual stress effects on fatigue life of welded structures using LEFM". *Engineering Failure Analysis*, Vol.: 16, pp. 449–467. Access: https://doi.org/10.1016/j.engfailanal.2008.06.017.

Colegrove, P.A., Ikeagu, C., Thistlethwait, A., Williams, S., Nagy, T., Suder, W., Steuwer, A., and Pirling, T., 2009. "Welding process impact on residual stress and distortion". *Science and Technology of Welding Joining*, Vol.: 14(8), pp. 717–726. Access: https://doi.org/10.1179/136217109X406938.

Cruz, M.F.N., 2022. *Estudo das Tensões Residuais nas Juntas de Aço 316L Soldadas por Processo LBW Utilizando Técnica Prism* (in Portuguese). Graduation Monography, Graduate Program in Mechanical Engineering, Federal University of Espirito Santo, Vitória, Brazil.

Edwards, L., 2006. "Influence of residual stress redistribution on fatigue crack growth and damage tolerant design". *Materials Science Forum*, Vol. 524–525, pp. 363–72. Access: https://doi.org/10.4028/www.scientific.net/MSF.524-525.363.

Feng, Y., Luo, Z., Liu, Z., Li, Y., Luo Y., and Huang, Y., 2015. "Keyhole gas tungsten arc welding of AISI 316L stainless steel". *Materials & Design*, Vol.: 85, pp. 24–31. Access: https://doi.org/10.1016/j.matdes.2015.07.011

Fundão, F.S., 2022. *Avaliação de tensões residuais em juntas sobrepostas soldadas por GTAW* (in Portuguese). Graduation Monography, Graduate Program in Mechanical Engineering, Federal University of Espirito Santo, Vitória, Brazil.

Gannon, L., Liu Y., Pegg N., and Smith M., 2010. "Effect of welding sequence on residual stress and distortion in flat-bar stiffened plates". *Marine Structures*, Vol. 23(3), pp. 385–404. Access: https://doi.org/10.1016/j.marstruc.2010.05.002

Hagenlocher, C., Wagner, J., Michel, J., Weber, R., Bachmann, M., Karadogan, C., Liewald, M., and Graf, T., 2020. *The influence of residual stresses on laser beam welding processes of aluminium sheets - Proceedings of 11th CIRP Conference on Photonic Technologies*, pp. 713-717. Access: https://doi.org/10.1016/j.procir.2020.09.124.

Haohui, X., Jose, A.F.O., Correia, B., Milan, V.C., Filippo, B.D., and Lance, M., 2021. "Residual stress effects on fatigue life prediction using hardness measurements for butt-welded joints made of high strength steels". *International Journal of Fatigue*, Vol.: 147. Access: https://doi.org/10.1016/j.ijfatigue.2021.106175.

Jiang, W., Zhang, Y., and Woo, W., 2012. "Using heat sink technology to decrease residual stress in 316L stainless steel welding joint: finite element simulation". *International Journal of Pressure Vessels and Piping*, Vol.: 92, pp. 56-62. Access: http://dx.doi.org/10.1016/j.ijpvp.2012.01.002.

Heinze, C., Schwenk, C., and Rethmeier, M., 2012. "Numerical calculation of residual stress development of multi-pass gas metal arc welding". *Journal of Constructional Steel Research*., Vol.: 72, pp. 12-19. Access: http://dx.doi. org/10.1016/j.jcsr.2011.08.011.

Jones, W.K.C. and Alberry, P.J., 1978. *The role of phase transformations in the development of residual stresses during the welding of some fast reactor steels - Proceedings of the International Conference on Ferritic steels for fast reactor steam generators*. In: British Nuclear Energy Society at the Institution of Civil Engineers. London: BNES; pp. 471-475. Access: http://dx.doi.org/10.1680/ fsffrsgv2.00490.0037.

Kumar, R., Ghosh, P.K., and Kumar, S., 2017. "Thermal and metallurgical characteristics of surface modification of AISI 8620 steel produced by TIG arcing process". *Journal of Materials Processing Technology*, Vol.: 240, pp. 420- 431. Access: http://dx.doi.org/10.1016/j.jmatprotec.2016.10.020.

Lee, C.K., Chiew, S.P., and Jiang, J., 2012. "Residual stress study of welded high strength steel thin-walled plate-to-plate joints. Part 1: experimental study". *Thin-walled Structures*. Vol.: 56, pp. 103-112. Access: http://dx.doi. org/10.1016/j.tws.2012.03.015.

Lee, H.W., 2007. "Weld metal hydrogen-assisted cracking in thick steel plate weldments". *Materials Science and Engineering*, Vol.: 445- 446, pp. 328-335. Access: http://dx.doi.org/10.1016/j.msea.2006.09.046.

Lin, Y.C. and Lee, K.H., 1997. "Effect of preheating on the residual stress in type 304 stainless steel weldment". *Journal of Materials Processing Technology*, Vol. 63(1-3), pp. 797-801. Access: http://dx.doi.org/10.1016/ S0924-0136(96)02727-6.

Liskevych, O., Almeida, E.M., Feijo, G. F., Macêdo, M. C. S., 2022. *Estudo de aplicabilidade da técnica ESPI (Electronic Specle Pattern Interferometry) combinada com o método do furo-cego para medição de tensões residuais em juntas soldadas (in Portuguese) – Proceedings of the XI Congresso Nacional de Engenharia Mecânica, CONEM 2022*, Teresina, Brazil;

Lu, J., 1996. *Handbook on measurement of residual stresses*. SEM - Society for Experimental Mechanics, The Fairmont Press, Lilburn, GA, USA.

Masubuchi, K., 1980. *Analysis of welded structures: residual stresses, distortion and their consequences*. New York: Pergamon Press; 1980. 641 p.

Mishchenko, A. and Scotti, A., 2018. "Residual stresses in arc welding: A holistic vision" (in Portuguese). *Welding & Inspection*, Vol.: 23(1), pp. 93–112. Access: https://doi.org/10.1590/0104-9224/SI2301.10.

Satoh, K., Terai, K., Ohkuma, S.Y., and Kinoshita, T., 1975. "Theoretical study on transient restraint stress in multi-pass welding". *Transactions of the Japan Welding Society*. Vol.: 6(1), pp. 42-52.

Scotti, A., 2014. "Modelos de cinco barras e de uma barra para geração de tensões térmicas na ZF, ZAC e MB durante soldagem a arco" (in Portuguese). *Soldagem e Inspeção*, Vol.: 19(1), pp. 82–90. Access: https://doi.org/10.1590/s0104-92242014000100010.

Schroepfer, D. and Kannengiesser, T., 2014. "Correlating welding reaction stresses and weld process conditions for high-strength steel S960QL". *Welding in the World*, Vol: 58(3), pp. 423-432. Access: http://dx.doi. org/10.1007/s40194-014-0127-x.

Schroepfer, D., Kromm, A., and Kannengiesser, T., 2017. "Engineering approach to assess residual stresses in welded components". *Welding in the World*, Vol. 61(1), pp. 91-106. Access: http://dx.doi.org/10.1007/ s40194-016-0394-9.

Soltani, H.M. and Tayebi, M., 2018. "Comparative study of AISI 304L to AISI 316L stainless steels joints by TIG and Nd: YAG laser welding". *Journal of Alloys and Compounds*, Vol. 767, pp. 112-121. Access: https://doi.org/10.1016/j.jallcom.2018.06.302.

Steinzig, M. and Ponslet, E., 2003. "Residual stress measurements using the hole drilling method and laser speckle interferometry - Part I". *Experimental Techniques*, Vol. 27(4), pp. 43–6. Access: https://doi.org/10.1111/j.1747-1567.2003.tb00114.x.

Steinzig, M. and Ponslet, E., 2003. "Residual stress measurements using the hole drilling method and laser speckle interferometry - Part II: Analysis technique". *Experimental Techniques*, Vol. 27(4), pp. 17–21. Access: https://doi.org/10.1111/j.1747-1567.2003.tb00117.x.

Sudheesh, R.S., Prasad, N.S., 2011. "Finite element study of residual stresses and distortions in arc welding with a trailing liquid nitrogen heat sink". *International Journal of Numerical Methods for Heat & Fluid Flow*, Vol. 21(8), pp. 1050-1065. Access: https://doi.org/10.1108/09615531111177787.

Teng, T., Fung, C-P., and Chang, P-H., 2002. "Effect of weld geometry and residual stresses on fatigue in butt-welded joints". *International Journal of Pressure Vessels and Piping*, Vol. 79(7), pp. 467-482. Access: http:// dx.doi.org/10.1016/S0308-0161(02)00060-1.

Upshaw, D., Steinzig, M., and Rasty, J., 2014. "Influence of Drilling Parameters on the Accuracy of Hole-drilling Residual Stress Measurements". *Experimental Mechanics*, Vol. 54(9), pp. 1537-1543. Access: https://doi.org/10.1007/s11340-014- 9923-x.

Vakili-Tahami, F. and Sorkhabi, A.H.D., 2009. "Finite element analysis of thickness effect on the residual stress in butt-weld 2.25Cr1Mo steel plates". *Journal of Applied Sciences*, Vol. 9(7), pp. 1331-1337. Access: http:// dx.doi.org/10.3923/jas.2009.1331.1337.

Vasantharaja, P., Maduarimuthu, V., Vasudevan, M., and Palanichamy, P., 2012. "Assessment of Residual Stresses and Distortion in Stainless Steel Weld Joints". *Materials Manufacturing*, Vol. 27, pp. 1376–1381. Access: https://doi.org/10.1080/10426914.2012.663135.

Xu, S., Wei, R., Wang, W., and Chen, X., 2014. "Residual stresses in the welding joint of the nozzle-to-head area of a layered high-pressure hydrogen storage tank". *International Journal of Hydrogen Energy*, Vol. 39(21), pp. 11061-11070. Access: http://dx.doi.org/10.1016/j. ijhydene.2014.05.066.

Zareie Rajani, H.R., Torkamani, H., Sharbati, M., and Raygan, Sh., 2012. "Corrosion resistance improvement in gas tungsten arc welded 316L stainless steel joints through controlled preheat treatment". *Materials and Design*, Vol. 34, pp. 51–57. Access: https://doi.org/10.1016/j.matdes.2011.07.071.